Int J Adv Manuf Technol (2018) 94:4125–4137
DOI 10.1007/s00170-017-1118-z

ORIGINAL ARTICLE

Research on the optimization mechanism of loading path in hydroforming process

Ying-ying Feng[1] · **Zong-an Luo**[1] · **Hai-long Su**[1] · **Qing-lin Wu**[1]

Received: 22 May 2017 / Accepted: 13 September 2017 / Published online: 30 September 2017

Abstract In this paper, the optimization mechanism of loading path in hydroforming process is researched. Firstly, the geometric model of an X-shaped tube is established by using 3D drawing software UG; the DYNAFORM software is used to simulate the forming performance of the X tube under different loading paths. The backward displacement is taken as the main factor of the loading path, and the loading path is presented in the form of three factor graphs; it can show the relationship of the main factors of the loading path visually, accurately, and precisely, which are axial feed, internal pressure, and back displacement. Secondly, the orthogonal test method is used to select the optimal loading path, and the back propagation (BP) neural network based on genetic algorithm is used to optimize the loading path of X tubes. Through synthetic consideration of the interrelation of the minimum wall thickness, the maximum wall thickness, the height of branch, and the contact area between branch tube and back punch, the average performance index function is established in the BP neural network control algorithm to optimize the learning efficiency and shorten the calculation time. Finally, verified by experiment, the optimization method of loading path for X tube hydroforming process could control the precision error of results between the simulation and the experiment within 5%, and has high accuracy and good feasibility.

Keywords Tube hydroforming · Loading path · Optimization algorithm · Average performance index function

✉ Ying-ying Feng
fengyy@ral.neu.edu.cn

[1] The State Key Laboratory of Rolling and Automation, Northeastern University, Shenyang 110819, China

1 Introduction

In recent years, in the face of energy shortage, environmental pollution, and a series of important issues with the development of human civilization in twenty-first century, lightweight technology is an effective way to reduce the vehicle weight, reduce fuel consumption, and improve environmental pollution. Because of its many advantages, the hydroforming technology of metal tubes has been paid more and more attention by researchers [1]. It takes tubes as processing objects to form complex geometry parts in one procedure and produce seamless composite tube and composite tube joint with high quality. It can reduce the weight of the part effectively, improve the production efficiency, reduce the subsequent machining and assembling welding, and improve the strength and stiffness of the parts. Recently, this technology is widely used to produce high-quality seamless tubes which are used in the air intake system, airplane pipeline system, train power system, sea pipeline system, the nuclear industry, and so on [2].

The final forming quality of metal tubes is affected by many factors such as axial feeding, internal pressure, backward displacement, material properties, friction, and mold structure. Meanwhile, various factors are mutual suppression and interconnected. Taking an X-shaped tube as an example, all the factors that control the tube form two-branch tubes to shape an X tube. If the internal pressure increases too fast, while the axial feed cannot be timely followed-up, the tubes are prone to excessive thinning or even rupture. On the contrary, if the axial feed is too large and the internal pressure increases slowly, it is easy to cause the accumulation of material in the mold cavity and to form a dead wrinkle finally. If the backward displacement (which is controlled by back punch) is too small, it will hinder the growth of the branch height. However, if the backward displacement is too large, it will cause the wall thickness to be reduced fast or even rupture

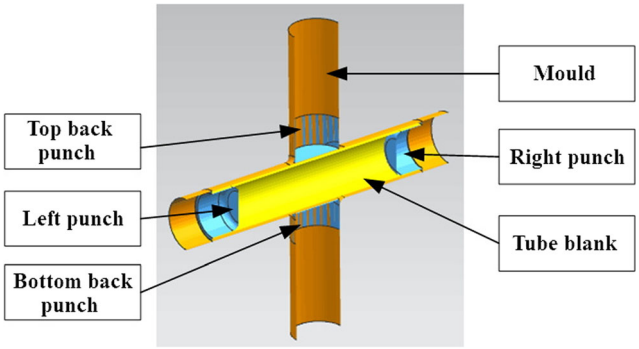

Fig. 1 The section of tube blank and mold

on the top of the branch. Meanwhile, it is restricted by the other factors of loading path [3, 4]. The qualified parts can be obtained only when the parameters are matched properly.

Many scholars in Germany, the USA, Japan, and other countries systematically studied the basic theoretical problems such as relationship between the failure mode and the loading path, the problem of forming interval, forming limit, wall thickness distribution, and material property test through theoretical analysiss, numerical simulation, and experiment. Kim et al. [5] predicted the forming limit of tube hydroforming through numerical analysis, which mainly studied the influence of loading path on forming results of aluminum alloy tube to form three-way tubes, and the relative experiment was compared to the theoretical analysis. Zadeh et al. [6] studied the influence of different loading paths on the wall thickness distribution of the three-way tube for general material. In addition, the results of numerical simulation were verified by experiments. Jain et al. [7] studied on the plastic stability of different kinds of coaxial variable diameter tubes for hydroforming, and the relationship between the critical equivalent ratio of strain and stress and material properties under different loading paths is deduced. Hwang et al. [8] studied the quantitative relationship among internal pressure, the friction coefficient, and the transition fillet radius of aluminum alloy variable diameter tubes during hydroforming process, and the applicability of the relation is proven by numerical simulation.

The mechanism, process, mold, and equipment of hydroforming were studied systematically by Professor Yuan et al. [9–13] at the Harbin Industrial University. According to the characteristics of deformation, the deformation law and elastic-plastic instability mechanism of thin shell were systematically studied. According to the general material such as stainless steel, low carbon steel, and aluminum alloy, the formation mechanism of the defects, the influence of loading path on the stress state, the distribution of wall thickness, and the filling behavior of fillet were revealed. DQSK low carbon steel was chosen as the material, and the numerical simulation was carried out to study the hydroforming process of the typical hollow member for the front beam of automobile by professor Xue and Zhou et al. [14, 15] at Hefei Industrial University. The results showed the forming process of wrinkling and fracture can be controlled by using the bilinear loading path with low-pressure clamping and high-pressure shaping together, and the final forming quality of parts was ideal. Professor Zhu et al. [16] systematically studied the hydroforming process of TRIP steel T tube, and the influence of the loading path on the formability, wall thickness distribution, and microstructure evolution of advanced high-strength steel tube was analyzed.

Many scholars study the effect of the loading path of tube hydroforming process on the properties of products for T tube, X tube, Y tube, and other typical tubes; however, the important parameter that is backward displacement will always be neglected because of the limitation of experimental conditions, which will lead to the loading path optimization results with only axial pressure and internal pressure are not ideal. On the other side, the design of the loading path is mostly cured on the set of single linear or bilinear curve, which will reduce the flexibility of the loading path on the formability of the product. So far, there is no consistent and clear conclusion about the intrinsic mechanism of the influence of loading path on the forming properties of tubes, and it lacks a set of loading path optimization scheme with strong universality which is available to various typical tubes. Therefore, studying the influence of loading path of hydroforming on the formability of tube, using intelligent control technology to find suitable loading paths for various shape parts, finding out the optimization mechanism of loading path, and perfecting the research system of tube hydroforming process have important significance to reduce the scrap rate of parts, cut the production costs, shorten the product development cycles, and spread the application of hydroforming technology [17–21].

In this paper, the geometric model of the X-shaped tube is established by using 3D drawing software UG, and DYNAFORM software is used to simulate the forming

Table 1 The unit type of each component

Component name	Grid type	Unit type	Unit numbers
Tube blank	Deformable body—shell element	Quadrilateral	13,703
Left and right punch	Rigid body—shell element	Quadrilateral	1294
Top and bottom back punch	Rigid body—shell element	Quadrilateral	662
Mold	Rigid body—shell element	Quadrilateral	5331

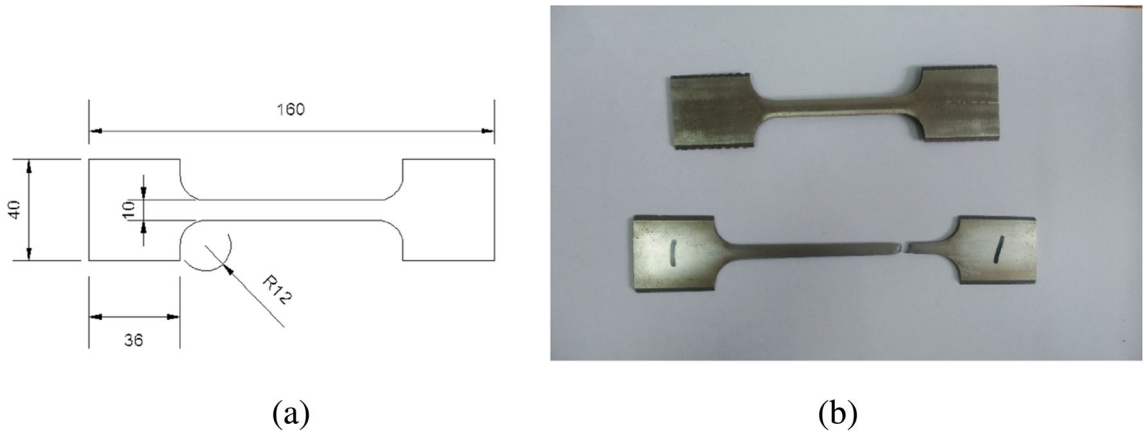

Fig. 2 **a**, **b** The drawing of the tensile sample size and practicality

performance of X tube under different loading paths firstly. Secondly, the orthogonal test and back propagation (BP) neural network based on genetic algorithm are used to optimize the loading path of X tubes. Finally, the accuracy and possibility of the loading path are verified by comparing with the experimental results.

2 The establishment of finite element model for X tube blank

Firstly, the geometric modeling of X tube with hydroforming is established by using 3D drawing software UG, and the IGES standard format is imported into the DYNAFORM software. Secondly, meshing of tube blanks, mold, and punches and setting boundary conditions are finished in DYNAFORM software, and the LS-DYNA is started to solve. Finally, the results are read into the DYNAFORM post-processor to analyze the results.

2.1 The establishment of geometric model of tube blank and mold

The thin shell elements are often used in the simulation of hydroforming; therefore, the slice model is adopted in the modeling, and the length of the tube blank is taken as 200 mm, the outer diameter is 42 mm, and the wall thickness is 1 mm. The section of the tube and the mold is shown in Fig. 1.

2.2 The meshing of X tube blank

The meshing of finite element model for X tube is divided into six parts: (a) tube blank, (b) mold, (c) left punch, (d) right punch, (e) top back punch, (f) bottom back punch. The punches are designated as discrete rigid body and the tube blank is set as deformable. The unit type of each component is shown in Table 1.

LS-DYNA dynamic explicit algorithm is used to calculate, and the research shows the dynamic explicit algorithm adopts proportionate reduction time which has little effect on the simulation accuracy, but it can significantly shorten the running time and improve the computational efficiency. Therefore, the scaled forming time is set as 0.01 s.

2.3 Determination of material properties

In order to simulate more accurately, the mechanical properties of SS304 stainless steel tube were measured to reduce the error of simulation. The tensile test at room temperature was measured according to the specifications of GB/T228-2002. After the tensile test specimen was made by wire cutting, the experiment was carried out on the INSTRON4206 electronic universal material-testing machine. The drawing of tensile sample size is shown in Fig. 2a, and the drawing of practical tensile sample is shown in Fig. 2b. In this paper, the material in the numerical simulation is chosen as SS304 stainless steel, which can be regarded as isotropic, and the specific performance parameters are shown in Table 2.

Table 2 Material property

Sample material	Yield strength /MPa	Tensile strength /MPa	Elongation /%	Hardening modulus *F*/MPa
304 stainless steel	374.6	658.74	53	2128

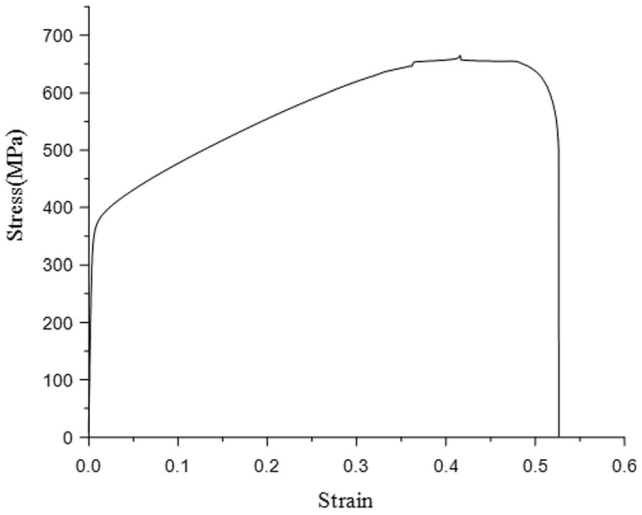

Fig. 3 The stress-strain curve of 304 stainless steel

After the experimental data are collected by equipment, the stress-strain curve drawn by Origin software is shown in Fig. 3.

3 Research on the intelligent control method to optimize loading path

The matching relationship of process parameters has a great influence on the forming results. Meanwhile, the backward displacement is added to compose the loading path, which makes the matching relationship of process parameters more complicated. Therefore, the intelligent control method is used to optimize the matching of the loading path's critical factors (including axial feed, internal pressure, and backward displacement). And the optimization of the loading path, the relevant parameters, and the forming results (including the maximum of wall thickness, the minimum of wall thickness, the height of branch, and the contact area between branch tube and back punch) are obtained to provide the basis for production practice [22, 23].

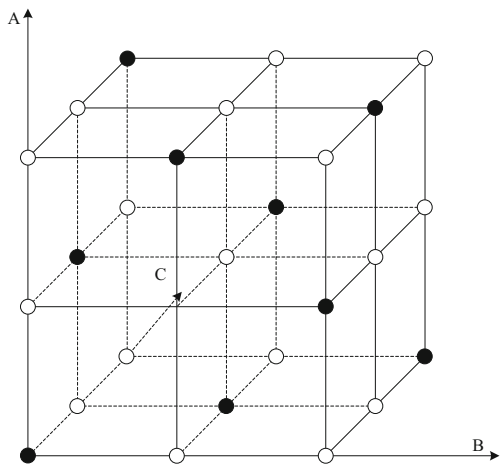

Fig. 4 The drawing of orthogonal test preferred area

3.1 The determination for the initial value of loading path

Some representative points are selected from the comprehensive experiment by the orthogonal experiment method, and the approach of three factors and three levels is selected. The three factors are axial feed, backward displacement, and internal pressure. Meanwhile, the three levels of each factor are defined as three reference values or three set paths, and the overall level of the combination of the three factors is $3^3 = 27$. The preferred area of the three factors is represented by cube in Fig. 4, and a total of nine trials were screened and expressed by "●". Each plane represents a level; there are a total of nine planes, each plane has three "●" points, and there is one "●" on each line of the cube, so the points are distributed in a balanced way. Therefore, the representativeness of the nine tests is strong, which can reflect the result of the experiment fairly comprehensive. It is reasonable to choose these nine loading paths as the initial values of the intelligent control method.

3.2 Research on the intelligent control method

The BP neural network based on the genetic algorithm has the ability of arbitrary nonlinear approximation, self-learning, and generalization, which enable the system to be adaptive, automatically adjust the control parameters, and improve the performance and reliability of the control [24–27]. Therefore, this intelligent control method is used to match and optimize the loading path (including axial feed, internal pressure, and backward displacement). And the forming results (including the maximum of wall thickness, the minimum of wall thickness, the height of branch, and the contact area between branch tube and back punch) are used to determine the rationality of the loading path.

The BP neural network structure is set up according to the optimization system of the loading path for hydroforming. The input layer of the three-layer BP neural network is:

$$Q_j^{(1)} = x(j) \quad (j = 1, 2, \ldots, \mathrm{M}) \tag{1}$$

In the formula, the number of input neurons M is selected as four, and the inputs are axial feed, internal pressure, backward displacement, and threshold. The inputs and outputs of the network hidden layer are:

$$net_i^{(2)}(k) = \sum_{j=1}^{M} \omega_{ij}^{(2)} \cdot Q_j^{(1)} \tag{2}$$

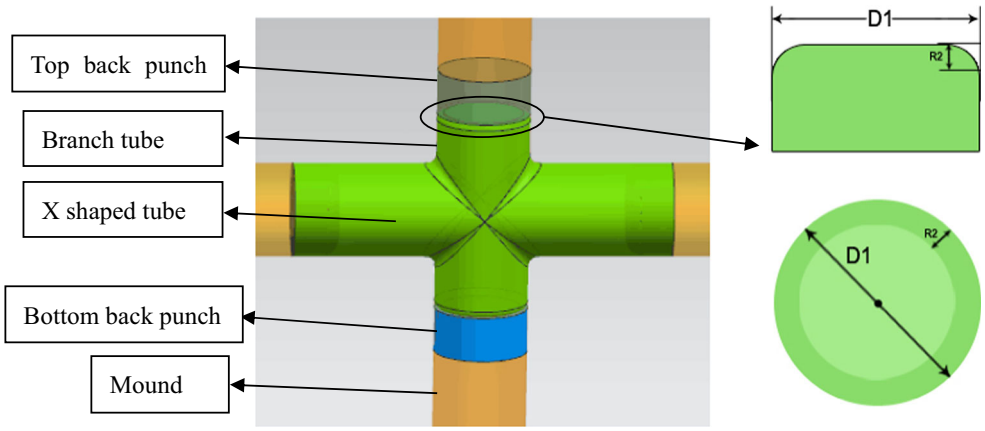

Fig. 5 The scheme of X shaped tube and contact area between the branch tube and back punch

$$Q_i^{(2)}(k) = f\left(\mathrm{net}_i^{(2)}(k)\right) \qquad (i = 1, 2, \ldots, \mathrm{Q}) \tag{3}$$

In formula, $\omega_{ij}^{(2)}$is the weighting coefficient of the hidden layer.

The inputs and outputs of the network output layer are:

$$\mathrm{net}_l^{(3)}(k) = \sum_{i=1}^{Q} \omega_{li}^{(3)} \cdot Q_i^{(2)}(k) \tag{4}$$

$$Q_l^{(3)}(k) = g\left(\mathrm{net}_l^{(3)}(k)\right) \qquad (l = 1, 2, 3) \tag{5}$$

$$Q_1^{(3)}(k) = T_{\max}, Q_2^{(3)}(k) = T_{\min}, Q_3^{(3)}(k) = H, Q_4^{(3)}(k) = S \tag{6}$$

The output nodes of output layer which correspond to the four adjustable parameters are $T_{\max}$ (the maximum of wall thickness), $T_{\min}$ (the minimum of wall thickness), H (the height of branch), and S (the contact area between branch tube and back punch).

The weights and thresholds of each layer for the BP network are cascaded in sequence by genetic algorithm, and N chromosomes are randomly generated. According to

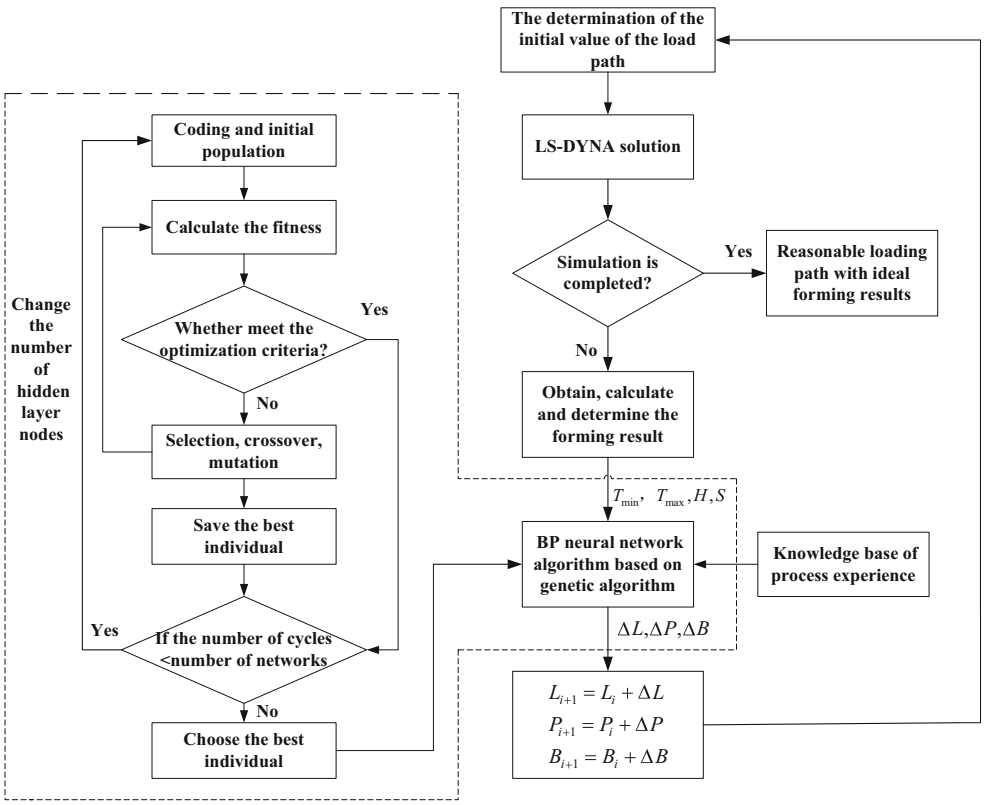

Fig. 6 Adaptive simulation and BP neural network control algorithm based on genetic algorithm

Table 3 Finite element simulation results of nine groups of loading paths selected by orthogonal test method

Forming performance loading path	1	2	3	4	5	6	7	8	9
Minimum wall thickness (mm)	0.661	0.667	0.133	0.766	0.367	0.260	0.708	0.609	0.651
Maximum wall thickness (mm)	2.262	2.228	2.217	2.215	2.167	2.129	2.103	2.052	2.035
The maximum thinning rate (%)	33.872	33.324	86.669	23.419	63.319	74.022	29.239	39.139	34.941
Branch height (mm)	26.677	22.603	28.719	22.654	28.727	26.670	28.668	26.632	22.619
The maximum principal strain	1.321	1.082	1.718	1.284	1.160	1.227	1.519	1.280	1.065
Contact area (mm^2)	806.56	894.03	–	1020.25	–	–	714.09	686.51	707.94

calculating the fitness, the crossover probability, and mutation probability, the ideal individuals are selected as initial weight and thresholds of BP network [28, 29]. The number of neurons in the hidden layer is five which is determined by genetic algorithm. Therefore, the neural network structure is determined as 4–5–4.

Evaluation rules of loading path are established according to the relevant technical experience under the premise of no cracking, buckling, wrinkle, and so on and need to meet the following requirements: (1) Making the minimum of wall thickness of tubes as much as possible. (2) Making the maximum of wall thickness of tubes as small as possible. (3) Making the wall thickness distribution more uniform. (4) Making the maximum of branch height of the tube as much as possible. (5) Making the contact area between the branch tube and back punch as large as possible.

The ideal range of maximum wall thickness, minimum wall thickness, branch height of the tube, and the contact area between the branch tube and back punch after hydroforming is determined according to different specifications of tube blanks. Meanwhile, performance index function is established according to T_{max}, T_{min}, H, and S.

$$E(k)_1 = \frac{1}{2}(r_1(k) - y_1(k))^2 \tag{7}$$

$$E(k)_2 = \frac{1}{2}(r_2(k) - y_2(k))^2 \tag{8}$$

$$E(k)_3 = \frac{1}{2}(r_3(k) - y_3(k))^2 \tag{9}$$

$$E(k)_4 = \frac{1}{2}(r_4(k) - y_4(k))^2 \tag{10}$$

$E(k)_1$, $E(k)_2$, $E(k)_3$, and $E(k)_4$ are the performance index functions corresponding to T_{max}, T_{min}, H, and S, respectively; $r_1(k)$, $r_2(k)$, $r_3(k)$, and $r_4(k)$ are the set values of T_{max}, T_{min}, H, and S of K cycle, and $y_1(k)$, $y_2(k)$, $y_3(k)$, and $y_4(k)$ are the feedback values of T_{max}, T_{min}, H, and S of K cycle.

Considering to correlate the ideal values of the above four factors, the average performance index function is:

$$E(k) = \frac{1}{4}\left(E(k)_1 + E(k)_2 + E(k)_3 + E(k)_4\right) \tag{11}$$

The weights of the network are modified according to the gradient descent method, and that is searched and changed according to the negative gradient direction of the weighting coefficient of $E(k)$. A tiny inertia term is added and it can fasten convergence on overall situation:

$$\Delta\omega_{li}^{(3)}(k) = -\eta \cdot \frac{\partial E(k)}{\partial \omega_{li}^{(3)}} + \alpha \Delta\omega_{li}^{(3)}(k\text{-}1) \tag{12}$$

In formula, η is the learning rate and α is the inertia coefficient.

Table 4 The parameters of loading paths A and B before optimization

Path A	Time (s)	Inter pressure (MPa)	Axial feed (mm)	Back displacement (mm)
	0	0	0	0
	0.001	30	2	1
	0.008	170	44	24
	0.01	190	46	26
Path B	0	0	0	0
	0.001	30	2	1
	0.008	130	44	26
	0.01	150	46	28

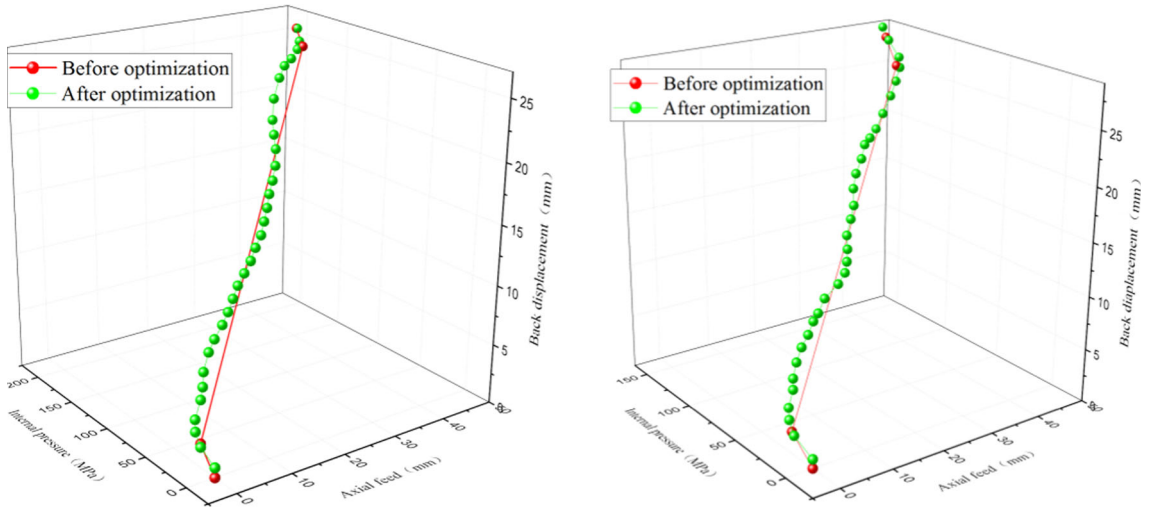

(a) Path A (b) Path B

Fig. 7 **a**, **b** Comparison chart of loading paths A and B before and after optimization

The learning algorithm of weighting coefficient for the network output layer is obtained as shown in Eqs. (13), (14), and (15), according to the classical incremental PID control algorithm and the above analysis.

$$\Delta\omega_{li}^{(3)}(k) = \alpha\Delta\omega_{li}^{(3)}(k-1) + \eta\cdot\delta_1^{(3)}\cdot Q_i^{(2)}(k) \quad (13)$$

$$\delta_l^{(3)} = error(k)\cdot\mathrm{sgn}\left(\frac{\partial y(k)}{\partial\Delta u(k)}\right)\cdot\frac{\partial\Delta u(k)}{\partial Q_l^{(3)}(k)}\cdot g'\left(\mathrm{net}_l^{(3)}(k)\right) \quad (14)$$

$$(l = 1, 2, 3)$$

$$g'(\cdot) = g(x)\cdot(1-g(x)) \quad (15)$$

Similarly, the algorithm of the weighting coefficient for the hidden layer will be obtained.

3.3 Application of the intelligent control method in finite element simulation

The above intelligent control method is programmed by Matlab software to obtain an independent subroutine, which is embedded in the solver (LS-DYNA) of DYNAFORM to complete simulation calculation. Firstly, the solution result of LS-DYNA is extracted by subroutine; the maximum of wall thickness, the minimum of wall thickness, the branch height of tube could be extracted directly; and the contact area between the branch and the back punch could be calculated by Eq. (16), which is determined by the diameter and the fillet radius of the branch tube that is obtained by fillet tangent from the profiles of the tube after hydroforming. The scheme of the X-shaped tube and contact area between branch tube and top back punch is shown in Fig. 5. For the symmetry, the contact area between the branch tube and bottom back punch is the same.

$$S=\pi\left(\frac{D_1}{2}-R_2\right)^2 \quad (16).$$

In formula, D_1 is the diameter of the branch tube, mm; R_2 is the fillet radius of branch tube, mm.

Secondly, by using the BP neural network controller, the load is adjusted according to the evaluation rules of loading path control; the genetic algorithm is used to search for the ideal solution. Finally, the load size of the *.Dyn file is modified and calculated by adaptive simulation. According to the above steps, the cycle calculation is carried out. When the results of forming parts (including the maximum of wall thickness, the minimum of wall thickness, the height of branch, and the contact area between the branch tube and back punch) meet the needs of calculation, the loading path will be obtained reasonably. For the flexible form of intelligent optimization, this optimization method could be used as the control technology of hydroforming for many kinds of other shape tubes. The flowchart of adaptive simulation and BP neural network control algorithm based on genetic algorithm is shown in Fig. 6. (In it, L is the axial feed, P is the internal pressure, B is the backward displacement.)

4 Results of finite element simulation

The finite element simulation calculation is carried out in the intelligent control system. According to the empirical formula [30], using the value of yield strength and tensile strength in Table 2, the initial yield strength of the tubes in the hydroforming process is set as 30 MPa, the maximum

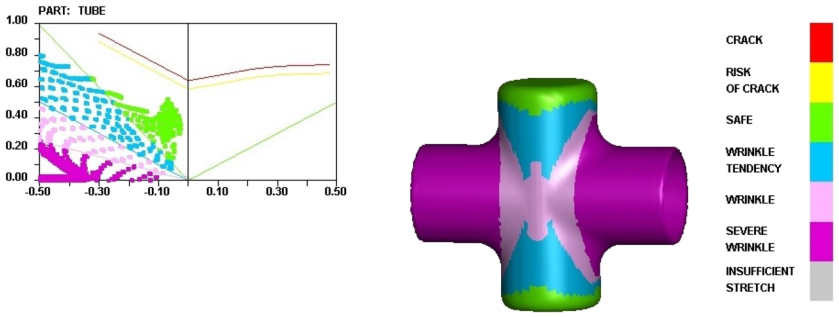

(a) Path A before optimization

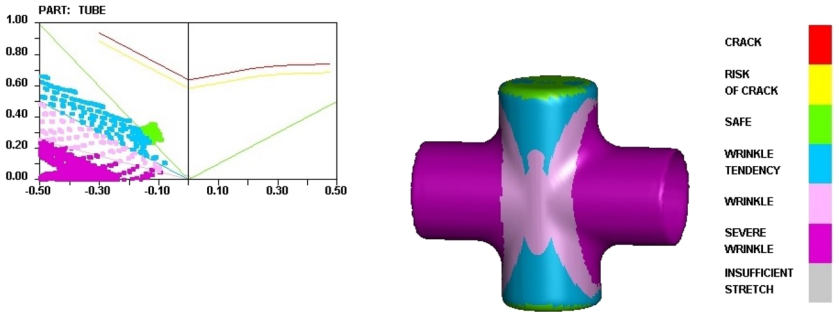

(b) Path A after optimization

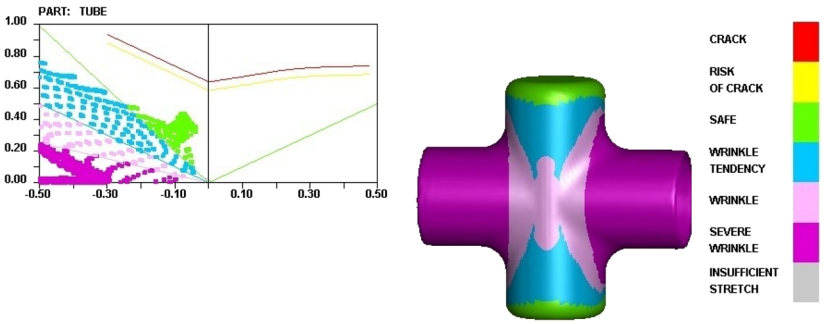

(c) Path B before optimization

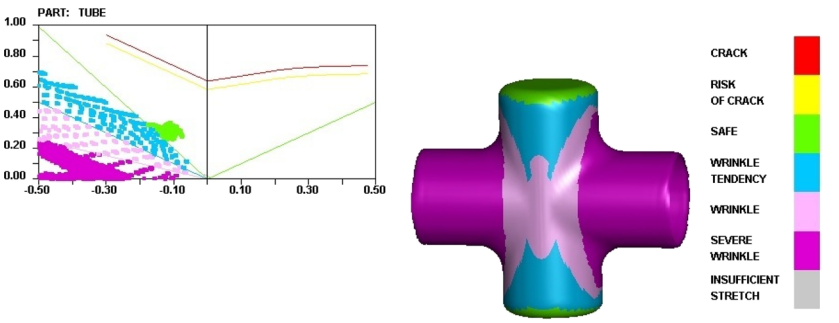

(d) Path B after optimization

Fig. 8 Tube hydroforming limit diagram of path A and path B before and after optimization. (**a**) Path A before optimization. (**b**) Path A after optimization. (**c**) Path B before optimization. (**d**) Path B after optimization

shaping pressure is 190 MPa, the maximum axial feed is 46 mm, and the maximum backward displacement is 28 mm. The nine groups of loading paths were screened by orthogonal test, and the results of finite element simulation are

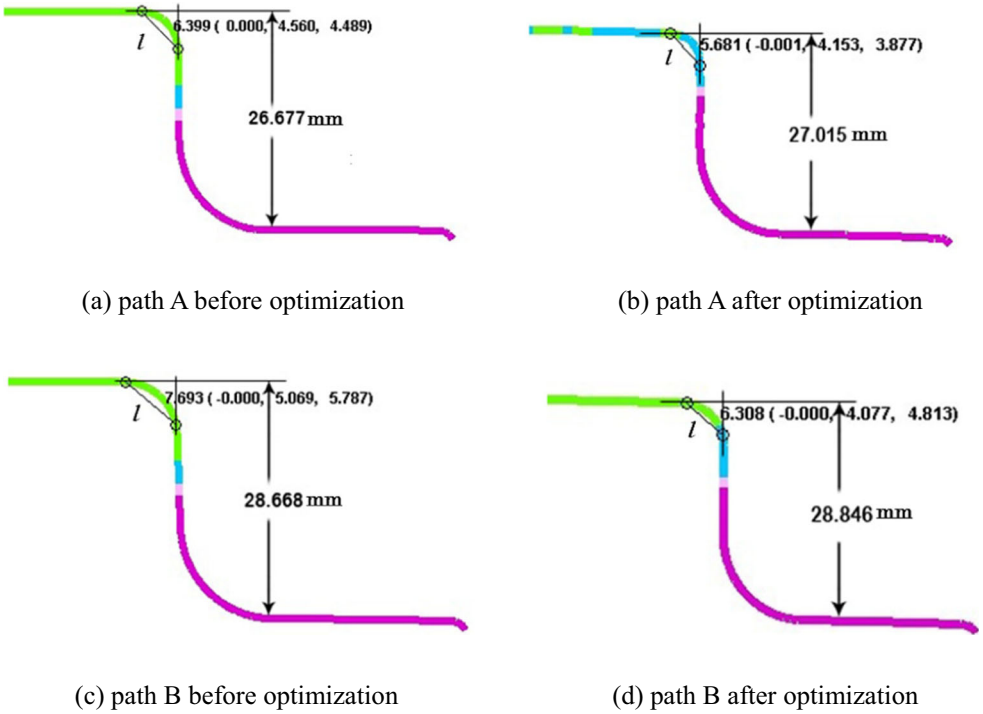

(a) path A before optimization

(b) path A after optimization

(c) path B before optimization

(d) path B after optimization

Fig. 9 The distance between two points of the fillet tangent and height of branch before and after optimization. **a** Path A before optimization. **b** Path A after optimization. **c** Path B before optimization. **d** Path B after optimization

shown in Table 3. From it, the maximum thinning rate of group 3, group 5, and group 6 is so large, which exceeds 50%, that the tube under these loading paths could rupture, so the results of the contact area cannot be calculated. Group 1 and group 7 are selected which have better formability and ideal height of branch tubes and are named as loading path A and B, which will be further optimized by adaptive simulation and BP neural network control algorithm based on genetic algorithm. The parameters of loading path A and B before optimization are shown in Table 4. The coefficient of friction between mold and tube is identified as 0.125 under simple single linear loading path, by comparing the results of simulation and experimental before all the research work [31]. Three factor curves of the loading path before and after optimization are shown in Fig. 7.

The backward displacement is taken as the main factor of the loading path, and the loading path is presented in the form of three factor graphs. Loading paths A and B are not the broken line after optimization, but the automatic adjustment curve around the paths before optimization, through adding control points according to the intelligent control method, the optimization criterion, and the formability, and they can adjust the loading paths adaptively. With the same axial feed, the back displacement of path B is larger than that of path A, while the internal pressure of path B is less than that of path A at the same time. Thus, in the hydroforming process, the growth of branch height under path B is faster than under path A, and the fillet radius of the branch tube is larger under path B. However, the maximum thinning rate of tube blank under path A is larger than under path B, because of the greater internal pressure. To get the smallest fillet radius of the branch tube and ensure the uniformity of tube wall thickness, the growth rate of the back displacement will be slowed down under path B, and the growth rate of internal pressure will be slowed down under path A during the process of loading path adaptive intelligent adjustment. At the same time, the adjustment with the other factors to optimize the forming results of tube blank can also be realized. The evolution trend of contrast curves of loading path before and after optimization is shown in Fig. 7a, b. Under the loading path before and after the optimization, the finite element simulation results of hydroforming are shown in Figs. 8, 9, 10, and 11 individually.

The comparison of the effect of loading paths before and after optimization of path A and path B on the formability of tube blanks can show that the optimized path A and path B play an important role in improving the formability of tube blank. The forming limit diagram can be seen from Fig. 8, and the optimized loading path makes the forming tendency of tube blank more reasonable, the feeding of both sides of the tube blank is more timely and enough. Under the optimized loading path, the blue area of the central part of the tube is obviously reduced, that is, the possibility of wrinkling and buckling deformation is reduced. Meanwhile, under the optimized loading path, the area of the green area on the top of the branch tube is significantly reduced, that means, the trend of cracking on

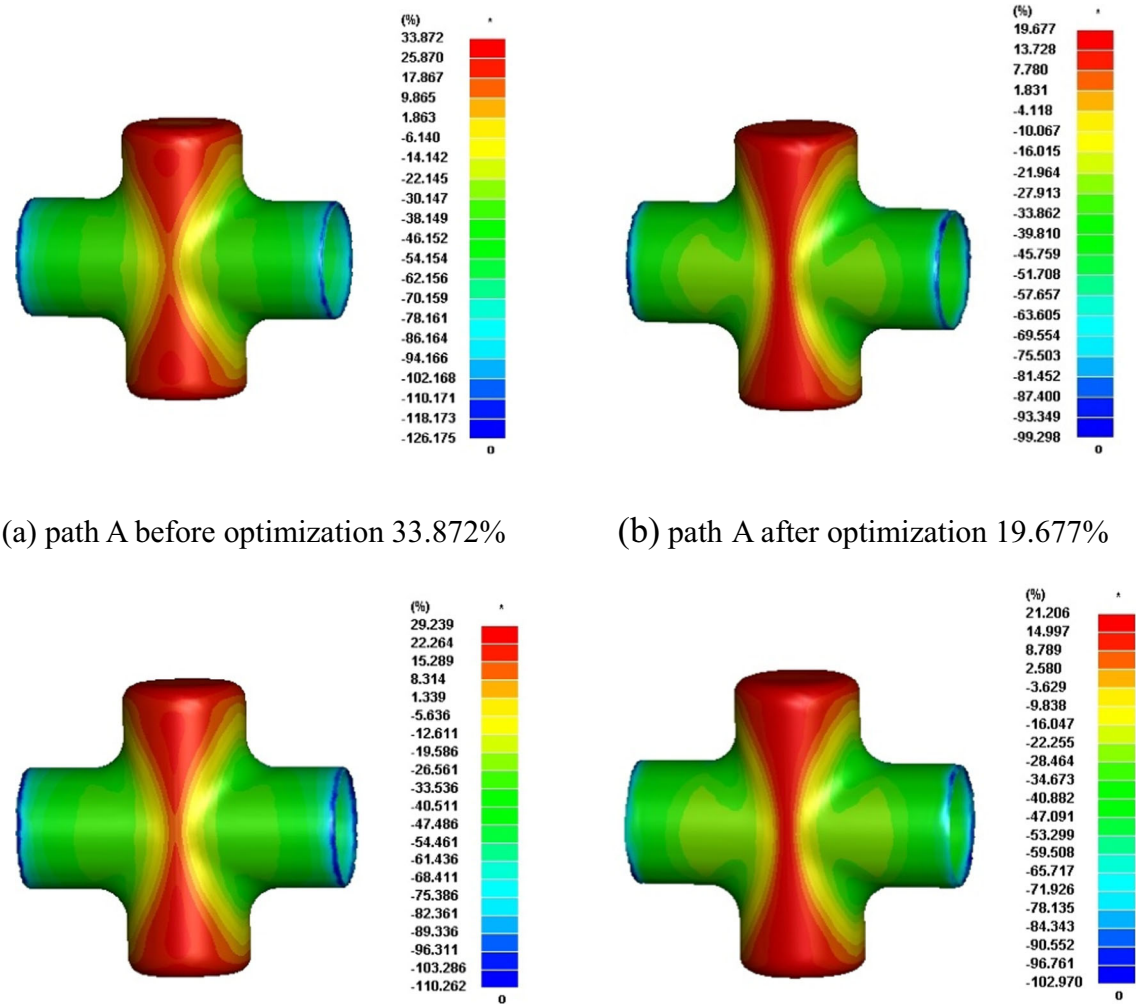

(a) path A before optimization 33.872%

(b) path A after optimization 19.677%

(c) path B before optimization 29.239%

(d) path B after optimization 21.206%

Fig. 10 The tube wall thickness distribution of path A and B before and after optimization. **a** Path A before optimization 33.872%. **b** Path A after optimization 19.677%. **c** Path B before optimization 29.239%. **d** Path B after optimization 21.206%

the top of the branch tube is effectively alleviated. The profiles of the tube after hydroforming are shown in Fig. 9; the contact of the branch tube and top back punch could also be observed. The fillet radius (R_2) of the branch tube is determined by measuring the distance (l) between two points of the fillet tangent. Meanwhile, the formula $R_2 = \frac{\sqrt{2}}{2} \cdot l$ is used to calculate the R_2 and to compare the contact of the branch tube and the top back punch between the loading paths before and after optimization. The fillet radius of the top edge of branch tubes under the optimized path A and path B is further reduced, the top edge of the branch tube is more fit with the punch, and the height of the branch tube is also better adjusted according to comparing the values of (a) and (b), (c) and (d) in Fig. 9, respectively.

The wall thickness distribution of path A and path B is known in Fig. 10. The optimized loading paths make the wall thickness distribution more uniform. The maximum thinning rate of the tube under path A is reduced from 33.872 to 19.677%, and the maximum thickening rate of the tube is reduced from 126.175 to 99.298%. Meanwhile, the maximum thinning rate of the tube under path B is reduced from 29.239 to 21.206%, and the maximum thickening rate of the tube is reduced from 110.262 to 102.970%. Therefore, the maximum and the minimum of wall thickness of the tube have been adjusted effectively under the optimized loading paths.

Under the optimized loading path, the distribution of the principal strain is also improved in the distribution curve of the principal strain in Fig. 11. The maximum principal strain is obviously improved, the maximum principal strain of path A is improved from 1.321 to 1.807, and the maximum principal strain of path B is improved from 1.519 to 1.773. However, the distribution area of the maximum principal strain is significantly reduced as

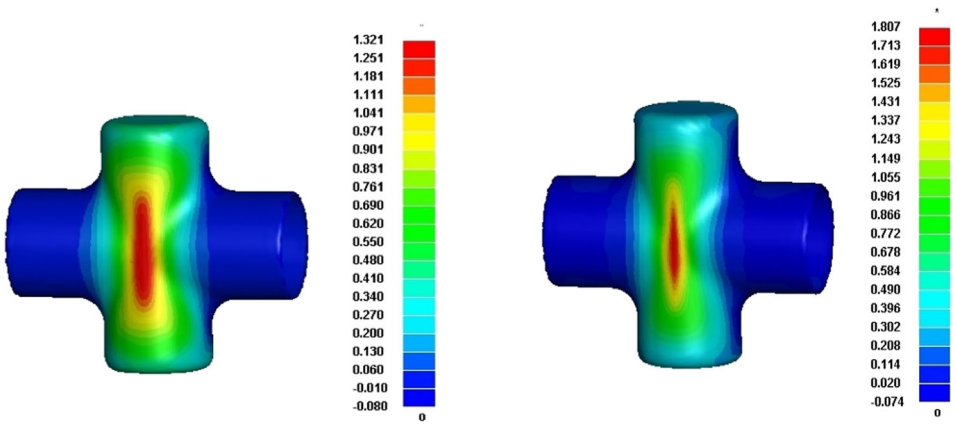

(a) path A before optimization 1.321 (b) path A after optimization1 1.807

(c) path B before optimization 1.519 (d) path B after optimization1.773

Fig. 11 The tube principal strain distribution of paths A and B before and after optimization. **a** Path A before optimization 1.321. **b** Path A after optimization1 1.807. **c** Path B before optimization 1.519. **d** Path B after optimization 1.773

shown with the red zone of Fig. 11, and the strain distribution of tube blanks is more uniform.

5 Experimental result

The intelligent control technology is applied to the laboratory-made 200-MPa hydroforming machine which is made by the State Key Laboratory of Rolling and Automation in Northeastern University, as is shown in Fig. 12. The results of path A and path B after optimization are both well; for the higher branch height of tube, the experimental test of the same process as the finite element simulation under path B is executed. Taking seven points to compare the difference, and the results of tube wall thickness and the height of branch tube for simulation and experiment are summarized in Table 5, and shown in Fig. 13a, b. From Table 5 and Fig. 13, the conclusion can be the experimental results well agree with the finite element simulation results, and the precision error of results between the

(a) Hydroforming machine (b) Mould and sample

Fig. 12 200 MPa hydroforming machine. **a** Hydroforming machine. **b** Mold and sample

Table 5 The wall thickness of simulation and experiment

Point position	No. 1 point	No. 2 point	No. 3 point	No. 4 point	No. 5 point	No. 6 point	No. 7 point
Wall thickness simulation value (mm)	0.992	1.135	1.378	1.458	1.596	1.539	1.554
Wall thickness actual value (mm)	0.963	1.102	1.439	1.525	1.642	1.592	1.616

simulation and the experiment could be controlled within 5% and has high accuracy and good feasibility, and for the comprehensive consideration of the method and the flexible form of intelligent optimization, the optimization method has wide applicability and could be used as the control technology of hydroforming for other similar shape tubes.

6 Conclusion

(1) The backward displacement is taken as the main factor of the loading path, and the loading path is presented in the form of three factor graphs; it can show the relationship of the main factors of the loading path visually accurately, and precisely, which are axial feed, internal pressure, and backward displacement. Meanwhile, the comparison between the loading paths before and after optimization can be shown in the diagram.

(2) The orthogonal test method is used to select the ideal loading path; this can reduce the mass screening work of the trial and error method effectively.

(3) Through synthetically considering the interrelation of the minimum wall thickness, the maximum wall thickness, the height of branch, and the contact area between branch tube and back punch, the average performance index function is established in the BP neural network control algorithm to optimize the learning efficiency and shorten the calculation time.

(4) The comparisons of the thickness distribution, the fillet radius, the height of the branch, and the principal strain distribution of the X tube before and after optimization show the orthogonal test method, adaptive simulation, and BP neural network control strategy based on genetic algorithm can solve the problem of matching and optimization of loading path which are internal pressure, axial feed, backward displacement, and the contact area between branch tube and back punch in the hydroforming process effectively.

(5) Verified by experiment, the optimization method of the loading path for X tube hydroforming process could control the precision error of results between the simulation and the experiment within 5% and has high accuracy and good feasibility, and for the comprehensive consideration of the method and the flexible form of intelligent optimization, the optimization method has wide applicability and could be used as the control technology of hydroforming for many kinds of other shape tubes.

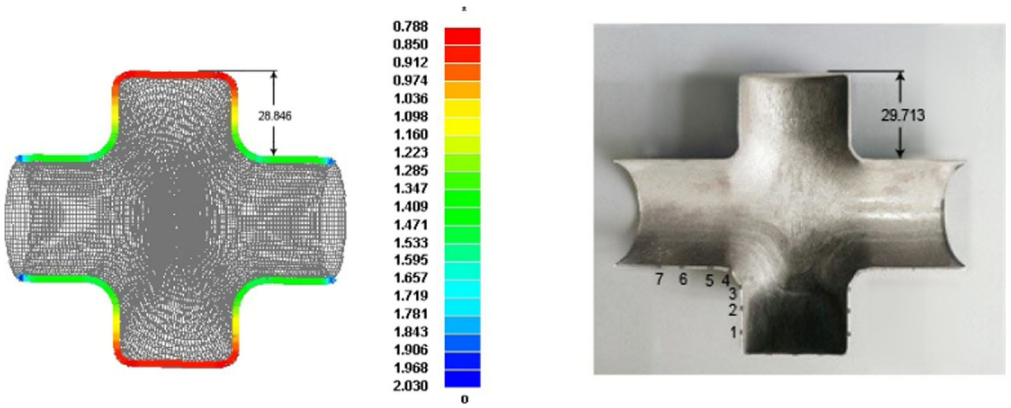

(a) The section thickness distribution chart of finite element simulation (b) Experimental sample section chart

Fig. 13 The section thickness distribution of finite element simulation and experimental sample section chart. **a** The section thickness distribution chart of finite element simulation. **b** Experimental sample section chart

Acknowledgements This work was financially supported by the Fundamental research funds for the Central Universities (N150704008) and National 863 Project (2015AA03A501-2).

References

1. Sorine M, Simha CHM, Riemsdijk IV, Worswick MJ (2008) Prediction of necking of high strength steel tubes during hydroforming-multi-axial loading. Int J Mech Sci 50:1411–1422
2. Ahmetoglu M, Altan T (2000) Tube hydroforming: state-of-the art and future trends. J Mater Process Technol 98:25–33
3. Alaswad A, Benyounis KY, Olabi AG (2012) Tube hydroforming process: a reference guide. Mater Des 33:328–339
4. Yang B, Zhang W, Li SH (2006) Analysis and finite element simulation of the tube bulge hydroforming process. Int J Adv Manuf Technol 29:453–458
5. Kim S, Kim Y (2002) Analytical study for tube hydroforming. J Mater Process Technol 128:232–239
6. Zadeh HK, Mashhadi MM (2006) Finite element simulation and experiment in tube hydroforming of unequal T shapes. J Mater Process Technol 177:684–687
7. Jain N, Wang J (2005) Plastic instability in dual-pressure tube-hydroforming process. Int J Mech Sci 47:1827–1837
8. Hwang YM, Chen WC (2005) Analysis of tube hydroforming in a square cross-sectional die. Int J Plast 21:1815–1833
9. Yuan SJ, Yuan WJ, Wang XS (2006) Effect of wrinkling behavior on formability and thickness distribution in tube hydroforming. J Mater Process Technol 177:668–671
10. Liu G, Yuan SJ, Teng BG (2006) Analysis of thinning at the transition corner in tube hydroforming. J Mater Process Technol 177: 688–691
11. Yuan SJ, Han C, Wang XS (2006) Hydroforming of automotive structural components with rectangular sections. Int J Mach Tools Manuf 46:1201–1206
12. Han C, Yuan SJ, Sun LN (2008) Reduction of friction and calibration pressure by section preform during hydroforming of tubular automotive structural components. Adv Mater Res 44-46:143–150
13. Teng BG, Hu L, Yuan SJ (2010) Deformation behavior of thin-walled tubes bending with internal pressure. Proc. of the 6th International Conference on Physical and Numerical Simulation of Materials Processing, Guilin, China, pp 528–534
14. Zhou L, Xue KM, Li P (2006) Study on hydroforming process of automobile front transom based on FEM. China Mech Eng 17:38–40
15. Xue KM, Zhou L (2006) Numerical simulation of hydroforming automotive front transom. Forging Stamping Technol 31:151–153
16. Liu JY, Zhang ZC, Manabe K, Li YM, Misra RDK (2014) Microstructure evolution of TRIP-aided seamless steel tube in T-shape hydroforming process. Mater Charact 94:149–160
17. An H, Green DE, Johrendt J (2012) A hybrid-constrained MOGA and local search method to optimize the load path for tube hydroforming. Int J Adv Manuf Technol 60:1017–1030
18. Abdessalem AB, EI-Hami A (2014) Global sensitivity analysis and multi-objective optimization of loading path in tube hydroforming process based on metamodelling techniques. Int J Adv Manuf Technol 71:753–773
19. Kadkhodayan M, Moghadam AE (2012) An investigation of the optimal load paths for the hydroforming of T-shaped tubes. Int J Adv Manuf Technol 61:73–85
20. Bihamta R, Bui QH, Guillot M, Amours GD, Rahem A (2015) Global optimization of the production of complex aluminium tubes by the hydroforming process. CIRP J Manuf Sci Technol 9:1–11
21. Huang TL, Song XW, Liu M (2016) The optimization of the loading path for T-shape tube hydroforming using adaptive radial basis function. Int J Adv Manuf Technol 82:1843–1857
22. Aue-U-Lan Y, Ngaile G, Altan T (2004) Optimization tube hydroforming using process simulation and experimental verification. J Mater Process Technol 146:137–143
23. Manabe KI, Suetake M, Koyama H, Yang M (2006) Hydroforming process optimization of aluminum alloy tube using intelligent control technique. Int J Mach Tools Manuf 46:1207–1211
24. Zhang FZ, Zhou QQ (2014) Ensemble detection model for profile injection attacks in collaborative recommender systems based on BP neural network. IET Inf Secur 9:24–31
25. Lin QQ, PENG DS, ZHU YZ (2005) Establishment of constitutive relationship model for 2519 aluminum alloy based on BP artificial neural network. J Cent S Univ Technol 12:380–384
26. Pan H, Wang XY, Chen Q, Huang SL (2005) Application of BP neural network based on genetic algorithm. Comput Appl 25:2777–2779
27. Ren T, Liu S, Yan GC, Mu HP (2016) Temperature prediction of the molten salt collector tube using BP neural network. IET Renew Power Gener 10:212–220
28. Song XW, Wu YF, Shen CL, Chen SM (2012) Test optimum design in three-way pipe hydroforming load path optimization. J Jilin Univ 42:57–61
29. Yang B (2011) Study on the loading paths of the tube hydroforming process. Doctoral Dissertation, Shanghai Jiao Tong University
30. Yuan SJ (2010) Lightweight forming technologies. National Defense Industry Press, China, pp 20–21
31. Chen FJ, Yang LF, Mao XC (2008) Approach of fiction measurement in expansion zone of tube hydroforming. Mod Machinery 5: 33–35